Ricin A-Chain: Kinetics, Mechanism, and RNA Stem−Loop Inhibitors†

Xiang-Yang Chen, Todd M. Link, and Vern L. Schramm*

Department of Biochemistry, Albert Einstein College of Medicine, 1300 Morris Park Avenue, Bronx, New York 10461

Received April 30, 1998; Revised Manuscript Received June 17, 1998

ABSTRACT: Ricin A-chain (RTA) catalyzes the depurination of a single adenine at position 4324 of 28S rRNA in a *N*-ribohydrolase reaction. The mechanism and specificity for RTA are examined using RNA stem−loop structures of 10−18 nucleotides which contain the required substrate motif, a GAGA tetraloop. At the optimal pH near 4.0, the preferred substrate is a 14-base stem−loop RNA which is hydrolyzed at 219 min^{-1} with a k_{cat}/K_m of 4.5×10^5 M^{-1} s^{-1} under conditions of steady-state catalysis. Smaller or larger stem−loop RNAs have lower k_{cat} values, but all have K_m values of ∼5 μM. Both the 10- and 18-base substrates have k_{cat}/K_m near 10^4 M^{-1} s^{-1}. Covalent cross-linking of the stem has a small effect on the kinetic parameters. Stem−loop DNA (10 bases) of the same sequence is also a substrate with a k_{cat}/K_m of 0.1 that for RNA. Chemical mechanisms for enzymatic RNA depurination reactions include leaving group activation, stabilization of a ribooxocarbenium transition state, a covalent enzyme−ribosyl intermediate, and ionization of the 2′-hydroxyl. A stem−loop RNA with *p*-nitrophenyl *O*-riboside at the depurination site is not a substrate, but binds tightly to the enzyme (K_i = 0.34 μM), consistent with a catalytic mechanism of leaving group activation. The substrate activity of stem−loop DNA eliminates ionization of the 2′-hydroxyl as a mechanism. Incorporation of the C-riboside formycin A at the depurination site provides an increased pK_a of the adenine analogue at N7. Binding of this analogue (K_i = 9.4 μM) is weaker than substrate which indicates that the altered pK_a at this position is not an important feature of transition state recognition. Stem−loop RNA with phenyliminoribitol at the depurination site increases the affinity substantially (K_i = 0.18 μM). The results are consistent with catalysis occurring by leaving group protonation at ring position(s) other than N7 leading to a ribooxocarbenium ion transition state. Small stem−loop RNAs have been identified with substrate activity within an order of magnitude of that reported for intact ribosomes.

Ricin A-chain (RTA) is an adenine-specific *N*-glycohydrolase, catalyzing depurination of stem−loop RNA which contains an invariable GAGA tetraloop motif (*1*). It has attracted increasing interest in recent years due to its potential applications in chemotherapy (*2*). The native substrate of RTA is eukaryotic 28S ribosomal RNA, which is depurinated at the remarkable rate of 1777 min^{-1} in intact ribosomes (*3*, *4*). RTA also catalyzes the hydrolysis of synthetic oligonucleotides as short as 10 bases provided that a base-paired stem and a GAGA tetraloop are present (*5*, *6*). With small stem−loop RNA substrates, the reported catalytic rate is decreased by as much as 6 orders of magnitude under the same conditions, and is highly dependent on assay conditions (*7*). In most reports of ricin A-chain activity at neutral pH and physiological ionic strength, the enzyme is incapable of multiple catalytic turnovers with small stem−loop RNAs. Multiple catalytic turnovers are required to define steady-state constants for substrates and inhibition constants for RNA analogues. In this report, a systematic investigation of the effects of reaction conditions on RTA hydrolytic activity, using RNA analogues and stem−loop RNA 10−18-mers as RTA substrates, has identified conditions for multiple catalytic turnovers which are within one-eighth the rate reported for native ribosomes (*4*). Oligonucleotide substrates and substrate analogues were characterized under optimal reaction conditions to establish RTA substrate and inhibitor specificity, and to provide an indication of the reaction mechanism (Figure 1).

Oligonucleotide RTA substrates containing a base-paired stem and the GAGA tetraloop motif have been structurally characterized by solution NMR studies (*8*, *9*). The results with both 5′-GGG UGC UCA GUA CGA GAG GAA CCG CAC CC-3′ and 5′-CUC AGA GAU GAG-3′ demonstrate tilted Watson−Crick base-pairing in the stem with an unusual base-pairing between the first G and second A in the tetraloop that enhances the stability of the hairpin architecture. The depurination-site adenine is external to the loop in a solvent-accessible location, exposed to RTA attack, while the other nucleotide bases are buried within the phosphodiester backbone by hydrogen-bonding and base-stacking. RTA interactions with the stem−loop substrate and the mechanism of hydrolysis are unresolved. X-ray crystallography and site-directed mutagenesis studies have identified several key residues in the active site of RTA which might be involved in catalysis (*10*). Arg180 and Glu177 are proposed to hydrogen-bond or protonate the leaving group (Arg180) and to stabilize the ribooxocarbenium ion (Glu177). These studies led to a model of the mechanism of hydrolysis which

† Supported by NIH Research Grant CA72444 and Contract DAMD 17-93-C-3051 from the U.S. Army.

* Corresponding author. Telephone: (718) 430-2813. Fax: (718) 430-8565. E-mail: vern@aecom.yu.edu.

S0006-2960(98)00990-8 CCC: $15.00
Published on Web 07/28/1998

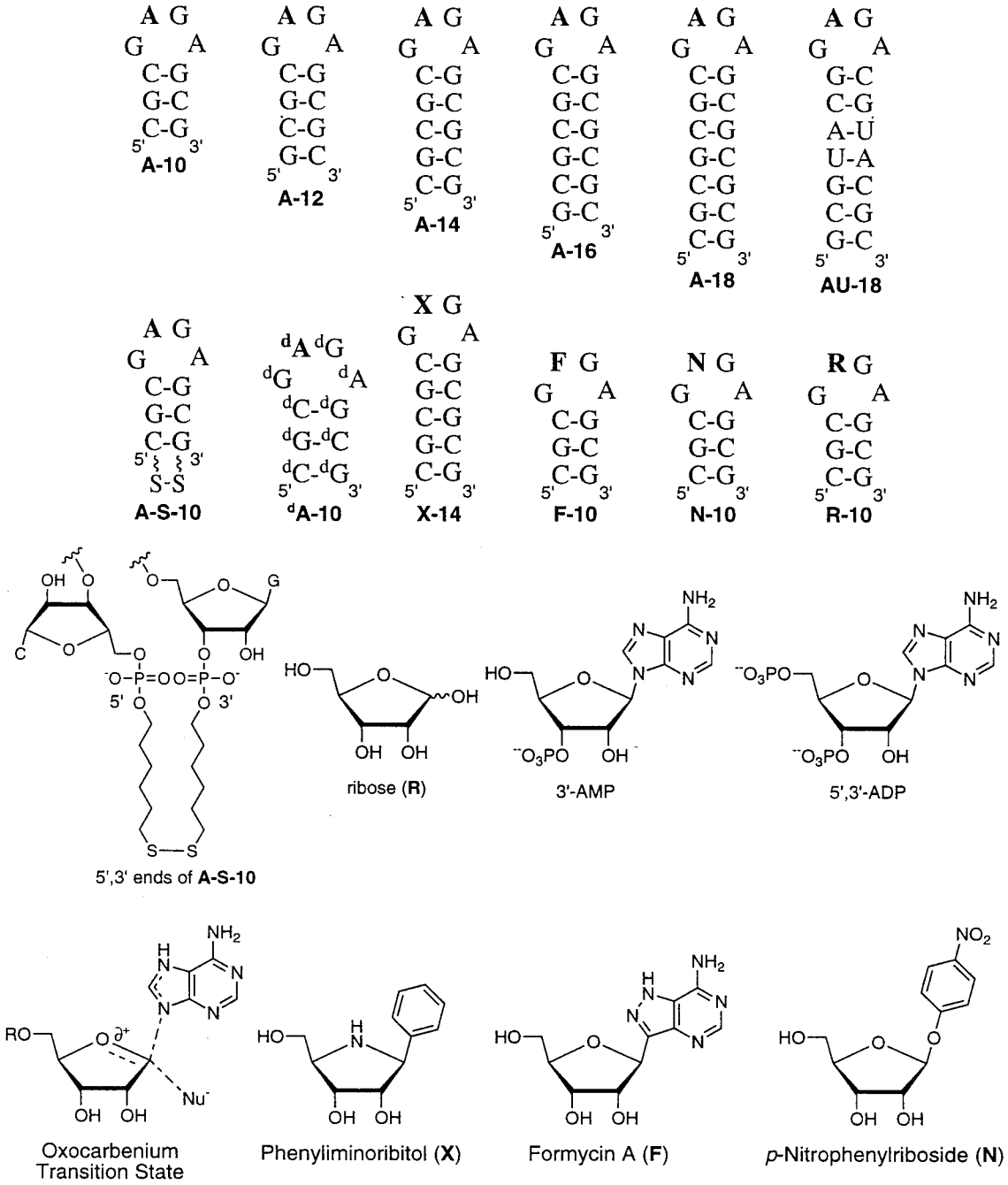

FIGURE 1: Structures of nucleosides, nucleotides, analogues, and stem−loop RNA and DNA used to characterize RTA. Chemical synthesis results in both the 5′- and 3′-termini of oligonucleotides being present as the hydroxyls. The ricin-susceptible adenine is shown in boldface type. Substituents incorporated into the RNA structures are indicated. The stem−loop DNA is indicated as ^{d}A-10. The structure "Oxocarbenium Transition State" is proposed from the known transition states of the closely related *N*-ribohydrolases, nucleoside hydrolase, and AMP nucleosidase (*12*).

suggested that RTA promotes hydrolysis through the well-known oxocarbenium ion transition state identified for other *N*-ribohydrolases (Figure 1) (*11*).

The oxocarbenium transition state of nucleoside and nucleotide *N*-ribohydrolase reactions has been extensively characterized by kinetic isotope effect studies, and tight-binding inhibitors have been designed by incorporating the major features of transition state structure into stable analogues (*12*, *13*). Substituted phenyliminoribitols and amidrazoneiminoribitols have been designed as transition-state analogue inhibitors of nucleoside hydrolases with K_i values to 2 nM (*14*, *15*). Formycin A monophosphate, a transition-state inhibitor of AMP nucleosidase, exhibits a K_i of 43 nM (*16*). Purine nucleoside phosphorylase is inhibited by 9-deazapurine analogues of 1,4-dideoxy-1,4-amino iminoribitols (*17*). These inhibitors are isozyme-specific since the enzymes reach the transition states by different mechanisms (*14*). Some *N*-riboside hydrolases activate the ribosyl group to the ribooxocarbenium ion while others activate the purine leaving groups (*18*). If RTA catalyzes depurination through an oxocarbenium transition state, its catalytic activity should be subject to inhibition by oxocarbenium mimics when placed in the suitable RNA structural context. In the present studies, synthetic oligonucleotides featuring substituents at the RTA depurination site were synthesized, and their interactions with RTA were investigated (Figure 1). These

results reveal insights on the mechanism of RTA catalysis, provide conditions which permit investigations under steady-state conditions of catalysis, and identify stem−loop RNA molecules which are of interest for further development of inhibitors with increased efficiency.

EXPERIMENTAL SECTION

Materials. Nucleoside and deoxynucleoside phosphoramidites and reagents for standard oligonucleotide synthesis were supplied by Applied Biosystems. 1-*O*-Dimethoxytritylhexyl disulfide, 1′-[(2-cyanoethyl)(*N*,*N*-diisopropyl)]phosphoramidite, was obtained from Glen Research. Other reagents were purchased from either Aldrich or Fischer. Phenyliminoribitol phosphoramidite, formycin A phosphoramidite, and *p*-nitrophenyl-*O*-riboside phosphoramidite[1] were prepared as described (*19*, *20*). Native and deglycosylated ricin A-chain was obtained from Sigma or Inland Laboratories (Austin, TX) or was purified from castor beans. Ricin A-chain produced from transformed *E. coli* was generously provided by Dr. Jon D. Robertus, University of Texas at Austin.

Synthesis of Oligoribonucleotides. Oligonucleotides were synthesized on the 1 μmol scale with an ABI 391 DNA/RNA synthesizer using standard phosphoramidite chemistry. The product was cleaved from solid support by treatment with concentrated ammonium hydroxide/ethanol (3:1) at room temperature for 2−3 h and then at 55 °C for 3−4 h to remove exocyclic amine protecting groups. The resulting ammonia/ethanol solution was dried thoroughly overnight under vacuum (Speedvac) to afford a residue to which was added neat triethylamine trihydrofluoride. The mixture was gently vortexed at room temperature for 1 day, quenched with water, and mixed with *n*-butanol. The crude oligonucleotide was precipitated at −20 °C and collected by centrifugation at 4 °C. Further purification of oligonucleotides was carried out by anion-exchange HPLC on a Nucleogen DEAE 60-7 column eluting with a linear gradient of ammonium acetate in 20% acetonitrile at a flow rate of 2 mL/min, and followed by desalting on a G-10 Sephadex column eluted with deionized water.

Incorporation of unnatural phosphoramidites followed the same protocol as described above except that (1) RNA containing *p*-nitrophenyl-*O*-riboside was cleaved from the solid support and deblocked by treatment with ammonia-saturated methanol to minimize decomposition of the *p*-nitrophenyl-*O*-riboside residue, (2) RNA containing a cross-linked disulfide bridge was prepared as previously reported (*21*), and (3) phosphorylation of oligonucleotides was conducted using Phosphalink amidite (*22*).

Kinetic Studies of Ricin A-Chain. The extent of RNA hydrolysis by RTA was measured by HPLC determination of the amount of adenine released. After incubation at 37 °C for an appropriate time, the reaction was stopped by the direct injection of the mixture onto a reversed-phase C18 analytic column (μ-Bondapak, Waters) with isocratic elution in 50 mM ammonium acetate (pH 5.0) containing 10% methanol, at a flow rate of 1 mL/min. The enzyme protein is retained on the guard column under these conditions, causing termination of the reaction. The adenine peak was monitored at 260 nm and compared to adenine standards treated with the same protocol. In initial rate experiments, the extent of RNA hydrolysis was less than 15% of the total. Product formation was shown to conform to initial rate conditions during this part of the reaction.

pH Effect Studies. RTA catalytic activity was determined as a function of pH using RNA A-10 as the substrate. Reaction mixtures containing 0.05−0.5 μM RTA and 2.0−100 μM RNA A-10 were buffered with 10 mM each of pyrophosphate, citrate, phosphate, and 1 mM EDTA, adjusted to the desired pH with KOH. After incubation at 37 °C for 10−30 min, samples were injected directly onto the HPLC, and the released adenine was determined by the area under the peaks, using adenine standards as the control.

Steady-State Kinetics. Reaction mixtures containing 0.5−50 μM substrate and 1.0 nM to 0.25 μM RTA in a solution buffered with 10 mM potassium citrate and 1 mM EDTA (pH 4.0) were incubated at 37 °C for 10 min. The amount of adenine formed was analyzed by HPLC. Separate studies of the extent of RNA hydrolysis as a function of time established that these conditions conformed to initial rate conditions.

RNA Thermal Denaturation. A solution containing 2 μM A-10 in 10 mM potassium citrate and 1 mM EDTA (pH 4.0) was heated while recording UV spectra. Curves of absorbance versus temperature were recorded at 260 nm with a heating rate of 1.0 °C/min on a UVIKON spectrophotometer. Thermodynamic parameters were obtained by fitting curves to a two-state model with the KaleidaGraph program.

Inhibitory Studies. Reaction rates were determined using RNA A-10 as the substrate in reaction mixtures containing 10 mM potassium citrate and 1 mM EDTA (pH 4.0). The concentration of inhibitor was varied while that of A-10 was fixed at a concentration near the K_m value. Initial reaction rates were analyzed by the rate of adenine formation as determined by HPLC. The apparent inhibitor dissociation constants, K_i, were calculated from the equation for competitive inhibition, assuming direct competition between substrate and inhibitors: $v = k_{cat}A/[K_m(1 + I/K_i) + A]$, where v = initial reaction rate, A = substrate concentration, K_m = Michaelis constant, I = inhibitor concentration, and k_{cat} = catalytic turnover number.

Depurinated Oligonucleotide. Stem−loop RNA A-10 (10 μM) in 20 μL of solution containing 10 mM potassium citrate and 1 mM EDTA at pH 4.0 was treated with 1 μM RTA at 37 °C for 2 h to effect complete depurination at the susceptible adenine site. To this was added 0.3 N NaOH, followed by incubation at the same temperature for 16 h. The resulting hydrolysate was neutralized with 0.3 N HCl. The solution was diluted with an equal volume of buffer containing 0.1 M Tris·HCl, pH 9.3, 2 mM $MgCl_2$, 0.2 mM $ZnCl_2$, and 2 mM spermidine, and treated with 1 unit of calf intestinal alkaline phosphatase (Promega) at 37 °C for an additional 2 h. The sample was injected onto a reversed-phase C18 analytic column with isocratic elution of 50 mM NH_4OAc (pH 5.0) containing 10% MeOH, at a flow rate of 1 mL/min. The HPLC eluent was monitored at 260 nm. Standards of cytidine, guanosine, adenosine, and adenine were used to determine the amounts of each component in the reaction mixture.

[1] Unpublished results, P. C. Tyler and R. H. Furneaux, Industrial Research Limited, Lower Hutt, New Zealand.

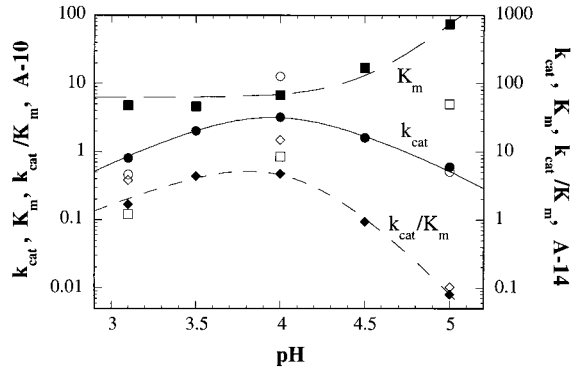

FIGURE 2: Kinetic constants for RTA as a function of pH using stem−loop RNA (A-10) as substrate (solid data points). The curves were fit to the equations $(k_{cat})_{app} = k_{cat}/[1 + H^+/K_{a1} + K_{a2}/H^+]$, $(K_m)_{app} = K_m[1 + (K_a/H^+)^2]$, or $(k_{cat}/K_m)_{app} = (k_{cat})_{app}/(K_m)_{app}$ (*23*). The lines were drawn as the best fits to these equations. The pK_a values obtained from the fits are given in Table 2. Kinetic constants obtained for A-14 stem−loop RNA at selected pH values are indicated by open symbols. For both A-10 and A-14, K_m = squares; k_{cat} = circles; k_{cat}/K_m = triangles.

Table 1: Michaelis−Menten Kinetic Constants of Substrates for RTA[a]

substrates	k_{cat} (min^{-1})	K_m (μM)	k_{cat}/K_m (M^{-1} s^{-1})
5′-AMP[b]	$<10^{-4}$	–	–
AG[b]	$<10^{-4}$	–	–
GAGA[b]	$<10^{-4}$	–	–
A-10	4.1 ± 0.3	4.1 ± 1.0	1.7×10^4
A-12	101 ± 7	2.7 ± 0.4	6.2×10^5
A-14	219 ± 14	8.1 ± 0.7	4.5×10^5
A-16	54 ± 9	6.0 ± 1.3	1.5×10^5
A-18	16 ± 1	6.1 ± 0.6	4.4×10^4
AU-18	0.76 ± 0.05	2.5 ± 0.5	0.6×10^4
A-S-10	2.6 ± 0.1	1.3 ± 0.3	3.4×10^4
[d]A-10[c]	0.38 ± 0.02	2.6 ± 0.4	0.3×10^4

[a] Kinetic constants were obtained from fits of the initial rate data vs substrate concentrations to the Michaelis−Menten equation. [b] RTA substrate activity on AMP, AG, and GAGA was tested at mono-, di-, and tetranucleotide concentrations of 1, 0.4, and 0.2 mM, respectively. Under these conditions, the lower limit of adenine detection corresponded to a rate of 10^{-4} min^{-1}. [c] Assay was performed in a solution buffered with 100 mM potassium acetate and 1 mM EDTA (pH 4.0).

RESULTS AND DISCUSSION

pH Dependence of Kinetic Constants for RTA. The hydrolytic activity of RTA was measured as a function of pH using A-10 as substrate. The kinetic parameters, K_m, k_{cat}, and k_{cat}/K_m, were found to be pH-dependent (Figure 2). The experimental data for k_{cat} were consistent with acid−base catalysis in which protonation of a site with pK_a 4.7 is required to form the active enzyme and protonation of a second group with pK_a 3.2 gives rise to inactive enzyme (Table 2). The bell-shaped curve for k_{cat} with unit limiting slopes indicates a single ionizable group responsible for both limbs of the pH profile. The K_m optimal value is 4 μM, and the K_m value is not influenced by increasing the H^+ concentration to pH 3.0. Increasing the pH causes a sharp increase in K_m, which indicates the titration of two groups with pK_a values near 4.5. In reactions where catalysis is slow relative to substrate binding and release, these K_m values can be interpreted in terms of substrate affinity. This condition applies to RTA and its interaction with A-10.[2] Crystallographic analyses of the RTA active site have implicated Glu177 and Asp96 as candidates for catalytic interactions based on mononucleotides bound in the catalytic site (*11*, *24*). Protonation of ionizable groups in RTA or in the RNA substrate with pK_a values near 4.5 could be responsible for these pH results. The N1 of adenine groups in RNA has a pK_a near 4 (*25*), and protonation of two adenines in the stem−loop structure could assist binding to RTA. Simple pH studies cannot resolve the issue of substrate or enzyme ionization, so the site of these groups must await other experimental approaches. The highest catalytic efficiency for RTA (k_{cat}/K_m) on A-10 RNA occurred within a narrow pH range with an optimal value near 4.0. A similar acidic pH value was also found to be the optimal pH for another ribosomal inactivating protein, saporin-L1 (*26*).

Table 2: pK_a Values for RTA with A-10 Substrate[a]

kinetic parameters	pK_{a1}	pK_{a2}	pK_a
k_{cat}	3.2 ± 1.4	4.7 ± 1.4	
K_m			4.5 ± 0.1
k_{cat}/K_m	4.1 ± 1.7	4.8 ± 1.7	4.0 ± 0.6

[a] The data of Figure 2 were fit to the equations defined in the legend to Figure 2 using the Curve Fit routine of KaleidaGraph. Graphical determination of pK_a values which are within 2 pH units is inaccurate, giving the relatively large errors observed for pK_a values associated with k_{cat} and k_{cat}/K_m. The pK_a value shown for K_m and k_{cat}/K_m is assumed to be two ionization sites with the same pK_a value.

The optimal stem−loop structure A-14 was examined over the pH range of 3−5 to determine if the pH optimum of 4 is an anomaly of small (A-10) stem−loops. The similar profile (Figure 2) establishes the low pH optimum for both A-10 and A-14. The pH optimum of 4.0 for the stem−loop RNAs differs from the RTA activity on ribosomes which is optimal at neutral pH (*27*). The low pH is apparently required to place the stem−loop RNA or RTA in the catalytically active ionization state or conformation. The catalytic competence of the RTA−ribosome complex at neutral pH indicates that structural components of the intact ribosome are necessary for efficient catalysis at physiological pH. At pH 4.0, A-10 remains in the base-paired structure as demonstrated from the thermal denaturation curve (T_m = ~60 °C). It is possible that a G·A interaction in the loop adopts an alternative conformation as a function of pH, such as G_{syn}-A^+_{anti}, rather than the interaction of the G_{anti}-A_{anti} form observed at neutral pH (*28*, *29*). The resulting RNA tertiary structure could more closely resemble the conformation of the stem−loop in 28S rRNA which is influenced by the extensive secondary structure of rRNA and the ribosomal proteins. The overall pH dependence is likely to be combination of ionization of substrate and enzymatic groups, and a conformational change of RNA tertiary structure. In subsequent studies, the RTA hydrolysis was conducted at the optimal pH of 4.0 for stem−loops under these assay conditions.

RTA Substrate Specificity. Stem−loop RNA 10-mer (A-10) is characterized by a K_m of 4.1 μM and a k_{cat} of 4.1 min^{-1}, to give a catalytic efficiency of 1.7×10^4 M^{-1} s^{-1} (Table 1). RTAs from three different sources, including the

[2] Substrate trapping and kinetic isotope experiments using labeled stem−loop RNA A-10 have demonstrated that the K_m for A-10 is within experimental error of the dissociation constant (X.-Y. Chen and V. L. Schramm, unpublished results).

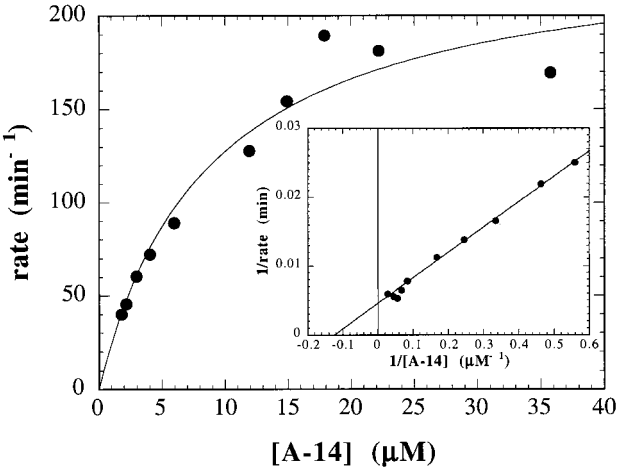

FIGURE 3: Substrate saturation curves and kinetic constants for hydrolysis of A-14 by RTA. The line in the main panel is the best fit of the data to the Michaelis−Menten equation. The line in the inset demonstrates the best fit of the data for A-14 hydrolysis to the double-reciprocal Michaelis−Menten equation.

native enzyme isolated from castor beans, the native enzyme which has been chemically deglycosylated, and the cloned A-chain overexpressed in *E. coli*, were characterized with A-10 as substrate. All enzymes gave similar kinetic parameters (results not shown). The K_m value of 4.1 μM is similar to that reported for RTA acting on ribosomes (*4*). The k_{cat} value of 4.1 min^{-1} is the largest turnover number reported for RTA with 10-base stem−loop RNA. The catalytic rate is greatest at pH 4.0, at low salt concentration, and in the presence of EDTA. However, k_{cat} is 400-fold lower than that reported for depurination of mammalian ribosomes. To investigate the effect of stem structure, RNA stem−loop structures A-10 to A-18 were tested (Figure 1). Variations were incorporated into the stem to investigate the effect of stem sequence. The catalytic turnover number increased to a maximum of 219 min^{-1} (Figure 3) with A-14 and decreased to less than 10% of that value at A-10 and A-18, respectively (Table 1). The K_m values vary only slightly from an average value near 5 μM. The maximum k_{cat} approaches one-eighth the value for RTA acting on native ribosomes (*4*). Although the k_{cat} approaches that for the physiological reaction, none of the substrates is active at pH 7.5.[3] The associated ribosomal components must therefore play a critical role in interacting with RTA and/or in orientating RNA stem−loop conformation optimally. Under the experimental conditions described here, multiple catalytic turnovers occurred, and complete hydrolysis of stem−loop RNA to the adenine depurinated product was obtained. The products of the reaction for A-10 were characterized by hydrolysis of depurinated oligonucleotide to individual monomer nucleosides which were analyzed by HPLC (see Experimental Section). Four UV-absorbing peaks in the HPLC profile corresponded to cytidine, guanosine, adenine, and adenosine, in a ratio of 3:5:1:1. Control substrate A-10 was also degraded to give three peaks as cytidine, guanosine, and adenosine (in a ratio of 3:5:2). The results demonstrated that RTA catalyzes the specific depurination of a single adenine from A-10 with the same specificity demonstrated by earlier studies using trace amounts of radiolabeled stem−loop RNAs at neutral pH.[4]

A-10 has been proposed to be the minimum substrate for RTA since it is the shortest oligonucleotide modified by RTA at physiological temperature. It has been proposed that shorter RNAs do not adapt a stable GAGA tetraloop (*6*). In aqueous solution, the linear monomer and dimer may coexist in a small fraction equilibrating with the active hairpin conformer. The catalytic efficiency of RTA might be improved on A-10 substrate if a more stable stem−loop structure is available. The stability of the RNA stem−loop structure can be enhanced by (1) increasing the length of stem, since the thermal stability of hairpin is directly proportional to the number of base pairs (*31*), and (2) tethering 3′- and 5′-termini of the oligonucleotide by disulfide cross-linking (*32*, *33*). AU-18 and A-18 were compared, and A-S-10 was synthesized and evaluated as substrates for RTA (Figure 1). Stem−loop RNA 8-mer 5′-CG GAGA CG-3′ cross-linked between the C bases by dithiols had been previously evaluated, and the substrate efficiency was improved 10-fold compared to that of non-cross-linked 8-mer (*34*). A-S-10 was tested as an RNA with cross-linkers between the 3′- and 5′-terminal ribosyls using bis(hexamethylene) disulfide. In the case of A-S-10, the values of K_m and k_{cat} were slightly reduced, compared to those of A-10. Therefore, increased stem stability has little effect on the kinetic parameters, and indicates that A-10 is fully base-paired during catalysis. This finding is incompatible with an earlier hypothesis that A-10 is a slow substrate at neutral pH values because of stem-melting at the catalytic site (*7*). Substitution of a stem structure with increased A-U content in the 18-base stem−loop (AU-18) decreased the k_{cat} by a factor of 20 (Table 1). Thus, the stem structure plays an important role in substrate specificity.

One mechanism for *N*-riboside depurination reactions proposes transition state formation following enzymatic ionization of the 2′-hydroxyl (*35*, *36*). To test this mechanism for RTA, stem−loop DNA 10-mer (^{d}A-10) was synthesized and tested as substrate (Figure 1). RTA catalyzes the hydrolysis of ^{d}A-10, with a K_m of 2.6 μM and a k_{cat} of 0.38 min^{-1} (Table 1). This finding is in contrast with an early report that a stem−loop DNA 32-mer which contained the sarcin/ricin loop was not a substrate for RTA (*30*). The K_m value is similar to that of A-10, and the k_{cat} drops 10-fold. In solution, stem−loop DNA with a GNNA tetraloop typically has a type I-loop and a B-form stem, while RNA with a GNRA tetraloop has a type III-loop and an A-form stem (Figure 4). The active site of RTA may accommodate structural differences between RNA and DNA, by reorganizing the nucleotide loop conformation that is required for

[3] At pH 7.5 and in the mixed buffer used for the pH profile, the reaction rates for A-12, A-14, and A-16 were less than 0.1% of the reaction rates at pH 4.0.

[4] At pH 7.5, incubation of 1.56 μM RTA and 2 μM RNA 35-mer from the sarcin/ricin domain of 28 S rRNA gave 10% conversion product after 1 h at 30 °C for a k_{cat} of 1 turnover per 7.8 h (*30*). The action of 1.65 μM RTA on 145 nM 5′-GGG GAGA CCC-3′ at 35 °C gave 10% depurination at 90 min for a k_{cat} of 1 turnover per 171 h under the same conditions (*6*). The k_{cat} of a 19-mer RNA sarcin/ricin domain (5′-GGGCACUCA GAGA UGAGUG-3′) was reported to be 0.71 min^{-1} at pH 7.0 at low ionic strength (*34*). Also at low ionic strength, 5′-CGC GAGA GCG-3′ was reported to have a k_{cat} of 1.7 min^{-1} with RTA at pH 7.5 (*19*). These rates of RTA action could not be reproduced at neutral pH values in this study, suggesting unstable control of pH by the low buffer concentrations used in the previously reported works.

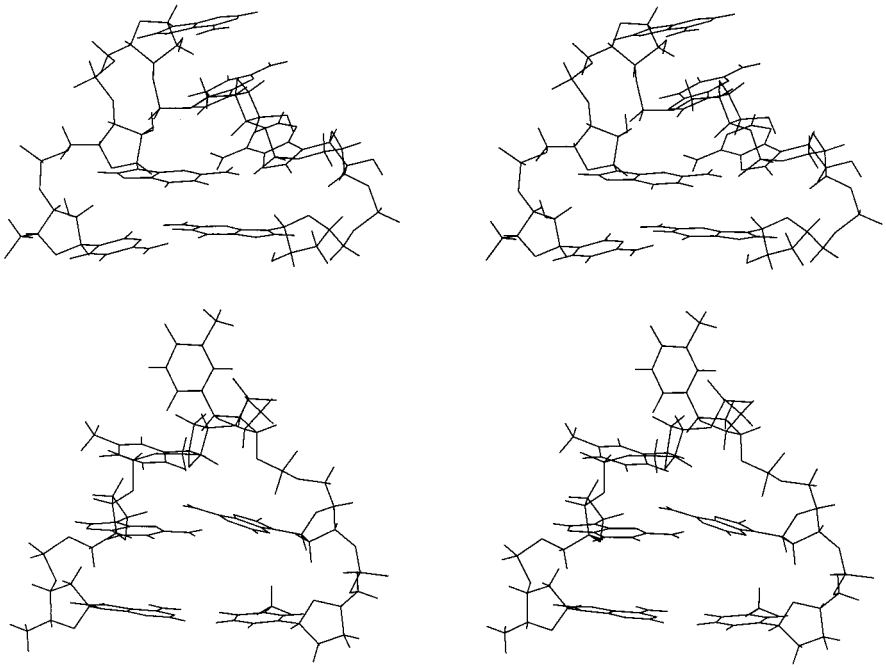

FIGURE 4: Stereoviews of stem−loop RNA (top, $^{5'}$C GAGA G$^{3'}$) and stem−loop DNA (bottom, $^{5'}$A GTTA T$^{3'}$). The drawings were created from the coordinates reported in references *37* and *38*, respectively.

catalysis. However, the equivalent K_m values for stem−loop RNA A-10 and DNA ^{d}A-10 indicate that the 2′-hydroxyl groups have little influence on substrate binding. The influence of the 2′-hydroxyl as the substrate for RTA can be further assessed with a stem−loop oligonucleotide with a G^{d}AGA tetraloop in which only the targeted adenosine has been replaced by 2′-deoxyadenosine, but the remainder of the polymer is RNA. Orita et al. recently reported that the oligonucleotide with stem-G^{d}AGA-stem has a similar overall solution structure as that with stem-GAGA-stem, and both were comparable RTA substrates (*39*). These results establish that ionization of the 2′-hydroxyl is not a significant interaction for C−N glycosidic bond scission. The 10-fold decrease in k_{cat} of ^{d}A-10 relative to A-10 may originate from the difference in solution structure or in the role that 2′-hydroxyl groups from other residues in the loop play in stabilizing the transition state complex. The nonessential role for the 2′-hydroxyl indicates that inhibitor design for RTA can be based on either the RNA or the DNA polymeric structure, thus providing altered stability toward nucleases.

Structural components of the tetraloop were also examined for substrate specificity. Adenosine, AMP, dinucleotide AG, and tetranucleotide GAGA were not hydrolyzed by RTA even in the presence of a stoichiometric excess of RTA relative to substrates (Table 1). It was previously reported that AMP could be cleaved by RTA during cocrystallization experiments (*40*), while AG binds weakly but is not hydrolyzed by RTA (*11*). The present results are in agreement with studies which indicated that RTA is catalytically active only on oligonucleotides with the stem−loop structural motif. The energy of activation for depurination by RTA is therefore obtained from the combined interactions between the enzyme and the substrate adenine as well as the adjacent GAGA tetraloop−stem structure. The susceptible C−N bond in adenosine or AMP residues alone is insufficient. Since the depurinated RNA 10-mer (R-10, Figure 1)[5] binds to RTA slightly better than A-10, most of the binding energy to form the Michaelis complex resides in portions of the stem−loop different from the susceptible adenine group (Table 3).

Table 3: Kinetic Constants of Inhibitors for RTA

inhibitor	K_i[a] (μM)
adenosine[b]	>5000
FMP[b]	>1000
5′-AMP[b]	>1000
3′-AMP[b]	>1000
3′,5′-ADP[b]	>1000
AG[b]	>1000
GAGA[b]	>400
R-10[c]	0.9 ± 0.1
N-10[c]	0.34 ± 0.06
F-10[c]	9.4 ± 0.7
X-14[c,d]	0.18 ± 0.02 (pH 4.0)
	25 ± 6 (pH 5.0)

[a] Inhibition studies used ~7 μM A-10 as substrate. [b] No inhibition was detected at maximum inhibitor concentrations of 0.2−2.5 mM. Maximum K_i values are reported as 2 × the highest tested inhibition concentration which gave no detectable inhibition. [c] K_i values were determined from fits of the initial rate data vs inhibitor concentrations to the expression $v = k_{cat}A/[K_m(1 + I/K_i) + A]$. [d] Previously reported at pH 7.5 and reported here at the indicated pH values (*19*).

Inhibition of RTA by RNA Stem−Loop Analogues. Oligonucleotides which feature distinct oxocarbenium transition state mimics at the RTA depurination site were chemically synthesized (Figure 1). Phenyliminoribitol (X) is known to mimic the developing oxocarbenium ion in the ribosyl ring of inosine in enzymes which are characterized by ribooxocarbenium ion transition states (*41*). Formycin A (F) monophosphate is a transition state analogue of AMP nucleosidase, an enzyme which depurinates AMP, chemistry similar to the RTA reaction (*42*). AMP nucleosidase acts by donating a proton to the adenine base prior to reaching

[5] R-10 was obtained by complete depurination of A-10 by RTA, followed by purification by HPLC using a reversed-phase C18 semi prep column.

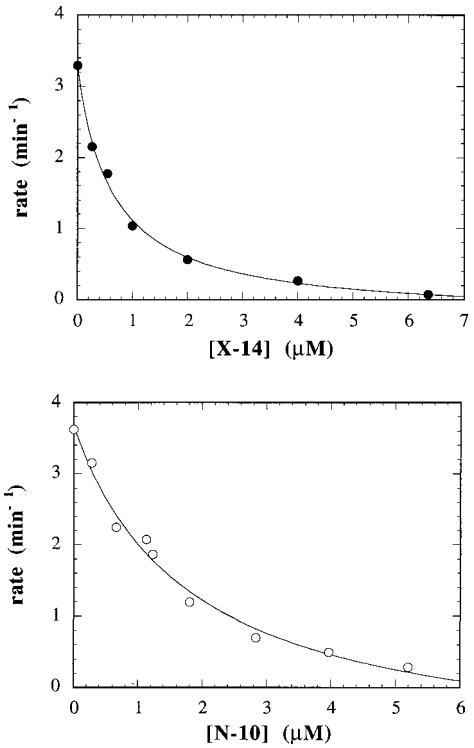

FIGURE 5: Inhibition of RTA by X-14 (upper panel) and N-10 (lower panel) using A-10 as the competitive substrate. The lines are the best fit of the data to the equation for competitive inhibition. The concentrations of A-10 were fixed at 7.3 and 6.9 μM, respectively.

the transition state. In formycin nucleotide, the elevated pK_a at the position corresponding to N7 in purine and a *syn*-ribosyl torsion angle are two features of the transition state for AMP nucleosidase (*43*). The formycin and iminoribitol analogues were incorporated separately into RNA stem−loop structures and were tested as RTA inhibitors using the stem−loop RNA 10-mer (A-10) as a competitive substrate. The phenyliminoribitol stem−loop (X-14) was described previously and tested at the unfavorable pH of 7.5 (*19*). At pH 4.0, X-14 and F-10 bind to RTA with K_i values of 0.18 and 9.4 μM, respectively (Table 2 and Figure 5). Phenyliminoribitol (X), formycin A monophosphate (FMP), adenosine, AMP, 5′,3′-ADP, AG, GAGA, dinucleotide pXGp, and tetranucleotides pGXGAp and GFGA showed no inhibitory activity against RTA at concentrations ranging from 200 μM to 2.5 mM (Table 3). The lack of inhibition by FMP at 200 μM is consistent with the observation from crystallographic studies that saturation of the catalytic site of RTA with FMP requires millimolar concentrations (*11*).

The interactions between RTA and several nucleotides and nucleotide analogues have been analyzed by X-ray crystallography (*11*, *40*). Tyr80 and Tyr123 are proposed to interact with the adenine ring by π-stacking, while Glu177 is proposed to stabilize the proposed developing oxocarbenium ion charge on the ribosyl ring by an electrostatic interaction. Protonation of Glu177 would eliminate the ability to ion-pair with the transition state and is consistent with the group of pK_a 3.3 seen in the pH profile for k_{cat}. The ring nitrogen in phenyliminoribitol has a pK_a of 6.5 (*41*). However, the neutral form of phenyliminoribitol has been proposed to be the active form of the inhibitor for interaction with nucleoside hydrolase (*44*). At pH 4.0, the iminoribitol is protonated, which mimics the positive charge developed at a ribooxocarbenium transition state. The K_i for X-14 with RTA was determined at both pH 4.0 and pH 5.0. The K_i value increased from 0.18 to 25 μM at the elevated pH (Table 3). The binding of X-14 decreases rapidly at increasing pH, consistent with multiple ionization sensitivity, as demonstrated for the K_m with A-10 (Figure 2). Thus, for RTA, the cationic form is implicated as the active inhibitor. However, ionization of several groups on the enzyme or X-14 at elevated pH caused a profound decrease in X-14 binding. The binding of X-14 to RTA could be achieved by electrostatic interaction of the protonated nitrogen of the iminoribitol ring with Glu177 and by favorable π-stacking of the phenyl ring between Tyr80 and Tyr123. Under the conditions for optimal catalytic activity, the binding affinity of X-14 to RTA is 23-fold stronger than that of the substrate, and 11 000 times tighter than the approximately 2 mM binding constant estimated for FMP (*11*). However, the inhibition constant is considerably weaker than expected for an efficient transition state analogue inhibitor. The energy required for the development of the proposed oxocarbenium ion transition state is contributed only partially from distortion of the ribosyl ring to the carbenium ion at the active site of the enzyme (*45*).

Analysis of Acid-Catalyzed Solvolysis. Another reaction pathway to an oxocarbenium transition state in *N*-ribosidic bond hydrolysis is protonation of the leaving group, a familiar mechanism in the acid-catalyzed solvolysis of nucleosides and nucleotides (*46*). Protonation of the leaving group has been theorized for RTA and can be tested in analogues with altered pK_a values in the leaving group. Formycin A is an isomer of adenosine in which the pK_a of the N7 position is elevated from that near 2 in adenosine to above 8 in formycin A (*47*). If protonation of the leaving group at N7 is involved at the transition state, stem−loop F-10 would be expected to bind favorably, as FMP does in AMP nucleosidase (*48*). F-10 binds to RTA approximately 2-fold weaker than substrate (Table 3), indicating that enzymatic protonation at N7 of the leaving group base is not a major contribution to transition state binding energy. The similar binding energies for A-10 and F-10 indicate that F-10 is a substrate analogue for RTA. All the nucleotide residues in stem−loop RNA have an *anti*-ribosyl torsion angle (*37*), while formycin A and FMP have *syn* conformations (*43*, *49*). This conformational preference of formycin A does not prevent the binding of F-10 to RTA. These results suggest that formation of an oxocarbenium transition state is facilitated by leaving group interactions at sites other than N7 and ribosyl ring activation. Inhibitors will require all of these features to be efficient transition state inhibitors. Another explanation for F-10 binding is that the increased pK_a at N7 of formycin A increases binding affinity but this interaction is canceled by an unfavorable binding energy for a nucleotide which has a preference for a *syn N*-ribosidic bond. Structural information will be required to resolve this question.

The mechanism of ribosyl versus leaving group activation in RTA riboside hydrolysis can be further explored by including a good leaving group at the position of the depurination site. An oligonucleotide containing *p*-nitrophenyl-*O*-riboside is diagnostic for ribosyl activation by RTA. If RTA catalysis occurs by leaving group activation, N-10 (Figure 1) would be a poor substrate since the

p-nitrophenyl group lacks a proton accepting site. If the enzyme acts by ribosyl activation to form the ribooxocarbenium ion transition state, N-10 would be an active substrate since the *p*-nitrophenoxyl group is an excellent leaving group. Ribosyl *N*-hydrolases which primarily activate the ribosyl group are known to hydrolyze *p*-nitrophenyl-*O*-riboside with a k_{cat}/K_m 58-fold greater than for the best of the natural substrates (*18*). Incubation of N-10 with RTA at pH 4.0 gave no detectable product under conditions which would have detected product formation at 10^{-5} the rate of A-10. In competition with A-10 as substrate, N-10 is a competitive inhibitor of the enzyme with a K_i of 0.34 μM (Table 3 and Figure 5). The lack of substrate activity therefore reflects a lack of catalytic activity rather than poor affinity for RTA. The substrate specificity indicates that a major factor in catalysis is leaving group activation, rather than activation of ribose to the oxocarbenium ion in stem−loop substrates.

Protonation of ring nitrogens in the adenine heterocycle facilitates departure of adenine. The results of crystallographic studies are controversial concerning the site of protonation. It was suggested that Arg180 is responsible for full or partial protonation of N3 of adenine (*11*, *45*). Results from site-directed mutagenesis supported this postulation (*50*). However, it was argued that Arg180 is close to Glu177, and can form an ion pair with Glu177 which would weaken its role in protonation. Asp96 has also been proposed as the proton-donating residue which interacts with N7 of the adenine ring instead (*24*). Protonation of this group is required to generate the catalytically active, proton-donating form of RTA, and is consistent with the required protonation of a group at pK_a 4.5 determined from the pH profile. The F-10 inhibition study indicates that N7 is unlikely to be the proton acceptor site. Structural studies, preferably with substrate and transition state analogues of stem−loop RNA, will be needed to resolve these issues. Based on the present studies, it is possible that nitrogens N1 and N3 of the adenine ring are protonated or involved in hydrogen bonding with RTA during catalysis. Multiple protonation is consistent with solution chemistry for the acid-catalyzed solvolysis of adenine nucleosides and nucleotides (*46*). Following activation of the leaving group, the adenine ring departs, forming an oxocarbenium ion at the transition state. The existence of the ribooxocarbenium ion at the transition state causes the iminoribitol analogue X-14 to bind well because of the oxocarbenium ion feature similar to the transition state. The closely related nucleoside hydrolases and AMP nucleosidase all stabilize ribooxocarbenium ion transition states which can also be proposed for RTA on the basis of increased affinity of the iminoribitol X-14.

CONCLUSIONS

Ricin A-chain catalyzes the adenine depurination of small stem−loop RNA at a rate up to one-eighth that for intact eukaryotic ribosomes. Optimal rates require pH 4 and a 14-base stem−loop with the GAGA tetraloop. The catalytic mechanism involves leaving group activation followed by ribooxocarbenium ion stabilization. Stem−loop RNA molecules with substituents at the ricin depurination site bind up to 20 times more tightly than substrate. These results demonstrate the robust catalytic activity of ricin A-chain on artificial RNA substrates and provide the means for detailed mechanistic studies of the depurinating plant toxin.

REFERENCES

1. Endo, Y., and Tsurugi, K. (1987) *J. Biol. Chem. 262*, 5908−5912.
2. Thrush, G. R., Lark, L. R., Clinchy, B. C., and Vitetta, E. S. (1996) *Annu. Rev. Immunol. 14*, 49−71.
3. Olsnes, S., and Pihl, A. (1982) in *Molecular Action of Toxins & Viruses* (Cohen, P., and van Heyningen, S., Eds.) pp 51−105, Elsevier Biomedical, New York.
4. Endo, Y., and Tsurugi, K. (1988) *J. Biol. Chem. 263*, 8735−8739.
5. Endo, Y., Chan, Y.-L., Lin, A., Tsurugi, K., and Wool, I. G. (1988) *J. Biol. Chem. 263*, 7919−7920.
6. Gluck, A., Endo, Y., and Wool, I. G. (1992) *J. Mol. Biol. 226*, 411−424.
7. Link, T., Chen, X. Y., and Schramm, V. L. (1996) *Toxicon 34*, 1317−1324.
8. Szewezak, A. A., Moore, P. B., Chan, Y.-L., and Wool, I. G. (1993) *Proc. Natl. Acad. Sci. U.S.A. 90*, 9581−9585.
9. Orita, M., Nishikawa, F., Shimayama, T., Taira, K., Endo, Y., and Nishikawa, S. (1993) *Nucleic Acids Res. 21*, 5670−5678.
10. Robertus, J. D., and Monzingo, A. F. (1996) in *Protein Toxin Structure* (Parker, M. W., Ed.) pp 253−270, Chapman & Hall, New York.
11. Monzingo, A. F., and Robertus, J. D. (1992) *J. Mol. Biol. 227*, 1136−1145.
12. Schramm, V. L., Horenstein, B. A., and Kline, P. C. (1994) *J. Biol. Chem. 269*, 18259−18262.
13. Schramm, V. L., Horenstein, B. A., Bagdassarian, C. K., Schwartz, S. D., Berti, P. J., Rising, K. A., Scheuring, J., Kline, P. C., Parkin, D. W., and Merkler, D. J. (1996) *Int. J. Quantum Chem.: Quantum Biol. Symp. No. 23*, 81−89.
14. Parkin, D. W., Limberg, G., Tyler, P. C., Furneaux, R. H., Chen, X. Y., and Schramm, V. L. (1997) *Biochemistry 36*, 3528−3534.
15. Boutellier, M., Horenstein, B. A., Semenyaka, A., Schramm, V. L., and Ganem, B. (1994) *Biochemistry 33*, 3994−4000.
16. DeWolf, W. E., Jr., Fullin, F. A., and Schramm, V. L. (1979) *J. Biol. Chem. 254*, 10868−10875.
17. Miles, R. W., Tyler, P. C., Furneaux, R. H., Bagdassarian, C. K., and Schramm, V. L. (1998) *Biochemistry 37*, 8615−8621.
18. Mazzella, L. J., Parkin, D. W., Tyler, P. C., Furneaux, R. H., and Schramm, V. L. (1996) *J. Am. Chem. Soc. 118*, 2112−2113.
19. Chen, X. Y., Link, T. M., and Schramm, V. L. (1996) *J. Am. Chem. Soc. 118*, 3067−3068.
20. Kuhn, H., Smith, D. P., and David, S. S. (1995) *J. Org. Chem. 60*, 7094−7095.
21. Gao, H., Yang, M., Patel, R., and Cook, P. F. (1995) *Nucleic Acids Res. 23*, 2025−2029.
22. User Bulletin 86, Applied Biosystems, Foster City, CA.
23. Segel, I. H. (1975) *Enzyme Kinetics*, Wiley & Sons, New York.
24. Huang, Q., Liu, S., Tang, Y., Jin, S., and Wang, Y. (1995) *Biochem. J. 309*, 285−298.
25. Legault, P., and Pardi, A. (1997) *J. Am. Chem. Soc. 119*, 6621−6628.
26. Barbieri, L., Valbonesi, P., Gorini, P., Pession, A., and Stirpe, F. (1996) *Biochem. J. 319*, 507−513.
27. Barbieri, L., Valbonesi, P., Bonora, E., Gorini, P., Bolognesi, A., and Stirpe, F. (1997) *Nucleic Acids Res. 25*, 518−522.
28. Morse, S. E., and Draper, D. E. (1995) *Nucleic Acids Res. 23*, 302−306.
29. Gao, X., and Patel, D. J. (1988) *J. Am. Chem. Soc. 110*, 5178−5182.
30. Endo, Y., Gluck, A., and Wool, I. G. (1991) *J. Mol. Biol. 221*, 193−207.
31. Puglisi, J. D., and Tinoco, I., Jr. (1989) *Methods Enzymol. 180*, 304−325.
32. Gao, H., Yang, M., and Cook, A. F. (1995) *Nucleic Acids Res. 23*, 285−292.

33. Goodwin, J. T., Osborne, S. E., Scholle, E. J., and Glick, G. D. (1996) *J. Am. Chem. Soc. 118*, 5207−5215.
34. Allerson, C. R., and Verdine, G. L. (1995) *Chem. Biol. 2*, 667−675.
35. Cherian, X. M., van Arman, S. A., and Czarnik, A. W. (1990) *J. Am. Chem. Soc. 112*, 4490−4498.
36. Handlon, A. L., Xu, C., Muller-Steffner, H. M., Schuber, F., and Oppenheimer, N. J. (1994) *J. Am. Chem. Soc. 116*, 12087−12088.
37. Jucker, F. M., Heus, H. A., Yip, P. F., Moors, E. H., and Pardi, A. (1996) *J. Mol. Biol. 264*, 968−980.
38. van Dongen, M. J. P., Mooren, M. M. W., Willems, E. F., van der Marel, G. A., van Boom, J. H., Wijmengal, S. S., and Hilbers, C. W. (1997) *Nucleic Acids Res. 25*, 1537−1547.
39. Orita, M., Nishikawa, F., Kohno, T., Senda, T., Mitsui, Y., Endo, Y., Taira, K., and Nishikawa, S. (1996) *Nucleic Acids Res. 24*, 611−618.
40. Weston, S. A., Tucker, A. D., Thatcher, D. R., Derbyshire, D. J., and Pauptit, R. A. (1994) *J. Mol. Biol. 244*, 410−422.
41. Horenstein, B. A., and Schramm, V. L. (1993) *Biochemistry 32*, 9917−9925.
42. Mentch, F., Parkin, D. W., and Schramm, V. L. (1987) *Biochemistry 26*, 921−930.
43. Giranda, V. L., Berman, H. M., and Schramm, V. L. (1988) *Biochemistry 27*, 5813−5818.
44. Parkin, D. W., and Schramm, V. L. (1995) *Biochemistry 34*, 13961−13966.
45. Ren, J., Wang, Y., Dong, Y., and Stuart, D. I. (1994) *Structure 2*, 7−16.
46. Garrett, E. R., and Mehta, P. J. (1972) *J. Am. Chem. Soc. 94*, 8532−8541.
47. Ward, D. C., Reich, E., and Stryer, L. (1969) *J. Biol. Chem. 244*, 1228−1237.
48. Ehrlich, J., and Schramm, V. L. (1994) *Biochemistry 33*, 8890−8896.
49. Koyama, G., Nakamura, H., and Umerzawa, H. (1976) *Acta Crystallogr. B32*, 813−820.
50. Day, P. J., Ernst, S. R., Frankel, A. E., Monzingo, A. F., Pascal, J. M., Molina-Svinth, M. C., and Robertus, J. D. (1996) *Biochemistry 35*, 11098−11103.

BI980990P